ARTICLE

$Mg_{0.58}Zn_{0.42}O$ Thin Films on MgO Substrates with MgO Buffer Layer

Shun Han,[†,‡] Jiying Zhang,[†] Zhenzhong Zhang,[*,†] Yanmin Zhao,[†] Likun Wang,[†] Jian Zheng,[†] Bin Yao,[†] Dongxu Zhao,[†] and Dezhen Shen[†]

Key Laboratory of Excited State Processes, Changchun Institute of Optics, Fine Mechanics and Physics, Chinese Academy of Sciences, 3888 Dongnanhu Road, Chang chun 130033, People's Republic of China, and Graduate School of the Chinese Academy of Sciences, Beijing 100039, People's Republic of China

ABSTRACT Cubic $Mg_{0.58}Zn_{0.42}O$ thin films with (100) orientation were grown on cubic MgO substrates. The band gap of the alloy films corresponds to solar blind band. In the case that a MgO buffer layer was employed, the surface roughness was decreased from 38 to 1.6 nm under the same growth conditions. A metal−semiconductor−metal photodetector based on this MgZnO film was fabricated, which showed a low dark current of 0.16 pA and lower sub-bandgap photoresponse than the ones with rougher surface in our early reports.

KEYWORDS: high smooth • MgZnO • MOCVD • UV photodetector

INTRODUCTION

Recently, solar-blind (200−280 nm) ultraviolet photodetectors have attracted more and more attention because of their application in missile warning, secure communications, flame sensing, etc. (1−4). Solid solar-blind ultraviolet photodetectors taking AlGaN alloys as a typical representative have got great improvements (5−8). However, because of the lack of lattice-matched substrate, high defect density of AlGaN thin films restricts the performance of AlGaN devices. MgZnO possess lattice-matched substrate and larger tunable band gap (3.3−7.8 eV) than AlGaN (3.6−6.0 eV) (9−12). It has shown greater potential on deep ultraviolet (DUV) photodetectors. Recently, MgZnO-based photodetectors with cutoff wavelengths almost covering the whole solar-blind region (225−287 nm) were reported, which were based on (111) orientation cubic MgZnO thin films grown on sapphire substrate (13). To further improve the quality of MgZnO, Peoples have attempted to introduce MgO buffer layer on heterosubstrates or use matched MgO substrate directly (14−16). As a corollary, it is foreseeable that it would get better crystal quality if the cubic MgZnO film is grown on MgO substrate with MgO buffer layer simultaneity, although few studies have been reported about it. In fact, similar growth processes have been used in GaAs films and devices for many years and it has been confirmed to be successful.

In this article, cubic MgZnO films were grown with MgO buffer layer on MgO substrate by metal−organic chemical vapor deposition technique. The surface smoothness was improved significantly. The MSM type solar-blind photodetector based on this MgZnO film shows lower sub-bandgap photoresponse.

EXPERIMENTAL SECTION

The MgZnO films were deposited on MgO (100) substrate by metal−organic chemical vapor deposition (MOCVD). Dimethyl dicyclopentadienyl magnesium (MCp_2Mg), diethyl zinc (DEZn) and oxygen with 5N purity (O_2) were employed as the precursors and nitrogen with 5N purity as the carrier gas. The deposition temperature was kept at 450 °C and the chamber pressure at 150 Torr. The flow rate of MCp_2Mg was fixed at 32.8 μmol/min, and DEZn at 10.7 μmol/min and O_2 at 0.086 mol/min, respectively. The thin film thickness is about 300 nm. The MgO buffer layer thickness is 25 nm.

The structural characterizations were carried out on a D/max-RA X-ray diffraction (XRD). The surface smoothness of the $Mg_xZn_{1-x}O$ thin films was characterized by a Di3100-s atomic force microscope (AFM). The surface morphology was characterized by a Hitachi S-4800 scanning electron microscope (SEM). The absorption spectra were measured on a Shimadzu UV-3101PC scanning spectrophotometer. The spectral response of the photodetector was measured using a 150 W Xe lamp, monochromator, chopper (EG&G 192), and lock-in amplifier (EG&G 124A). The current−voltage ($I-V$) characteristic of the MSM MgZnO-based photodetector was measured by a semiconductor parameter analyzer (Keithely 2200).

RESULTS AND DISCUSSION

Figure 1 shows the XRD $\theta-2\theta$ patterns of $Mg_xZn_{1-x}O$ thin films on MgO substrate without and with MgO buffer layer. For the $Mg_xZn_{1-x}O$ film without MgO buffer layer (curve A), a (200) diffraction of $Mg_xZn_{1-x}O$ appears at 42.52° besides the (200) diffraction peak of MgO substrate. Lattice constant (a_1) of cubic $Mg_xZn_{1-x}O$ is calculated to be 0.424 nm from Bragg equation ($n\lambda = 2d\sin\theta$, $a_1 = d/\sqrt{h^2 + k^2 + l^2}$). The lattice mismatch between the $Mg_xZn_{1-x}O$ thin film and MgO substrate is about 5%. The Mg composition of the sample is 58% calculated from eq 1, which is the dependence of the

* Corresponding author. E-mail: exciton@163.com. Tel: +86-43186176312. Fax: +86-43186176298.
Received for review March 22, 2010 and accepted June 28, 2010
† Key Laboratory of Excited State Processes, Changchun Institute of Optics, Fine Mechanics and Physics, Chinese Academy of Sciences.
‡ Graduate School of the Chinese Academy of Sciences.
DOI: 10.1021/am100249a

Published on Web 07/12/2010

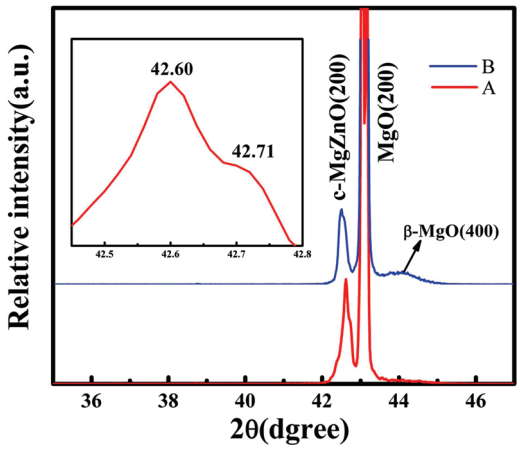

FIGURE 1. XRD spectra of MgZnO thin films on MgO substrate (A) without and (B) with MgO buffer layer.

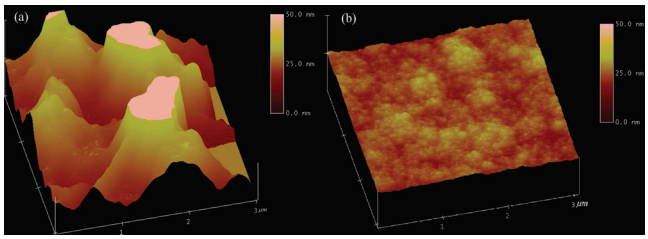

FIGURE 2. AFM images (3 × 3 μm^2) of $Mg_xZn_{1-x}O$ films (a) without and (b) with MgO buffer layer.

bond length as a function of composition assuming a virtual crystal of cubic MgZnO based on the Vegard's law (15).

$$l(Mg_xZn_{1-x}O) = x(2.106) + (1 - x)(2.14)\ (l = a/2) \quad (1)$$

Besides the MgZnO (002) peak, a new wide peak appears at 44.4°, which is corresponds to the diffraction of MgO (400) with a cubic spinel structure with a lattice constant of 8.12 Å (16). The cubic spinel phase come from the mix of MgO and $Mg(OH)_2$ (17), where the hydrogen should be from metal−organic precursors. For the $Mg_xZn_{1-x}O$ film with MgO buffer layer (curve B), the (200) peaks of $Mg_xZn_{1-x}O$ thin films shows a complex line shape. The amplificatory pattern is exhibited in the insert of Figure 1, where two clear peaks located at 42.60 and 42.71° corresponding to Kα1 and Kα2 can be observed. The diffraction of the cubic spinel MgO phase is suppressed significantly, which only leaves some vestige just differentiable from the baseline. From the above results, it can be concluded that MgO buffer benefits the crystal quality of cubic $Mg_xZn_{1-x}O$ thin film and restricts the occurrence of cubic spinel structure MgO. Besides the difference in crystal quality, the peak of the sample with buffer layer shifts to large angle side compared to that without buffer. It means that Mg composition is increased a little when MgO buffer layer was employed, although the growth parameters are the same.

The AFM images with 3 × 3 μm^2 area of the samples are shown in Figure 2. It is seen that the surface smoothness is improved significantly after MgO buffer was used. The rms

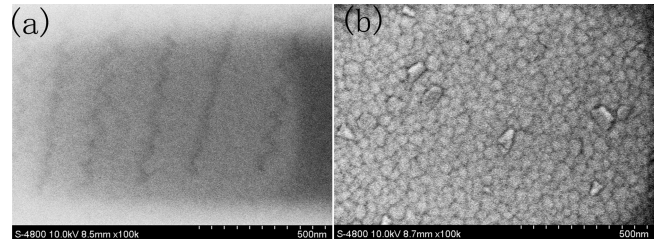

FIGURE 3. Surface SEM images of MgO substrates (a) without and (b) with MgO buffer layer.

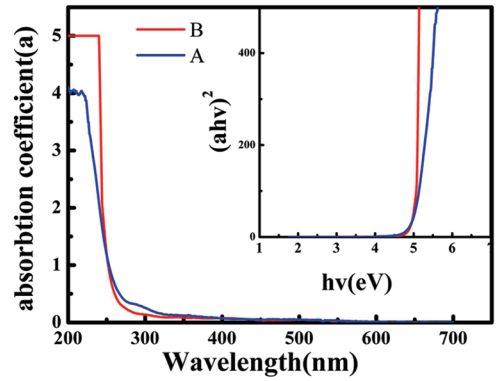

FIGURE 4. Optical absorption spectra of the $Mg_xZn_{1-x}O$ films on MgO substrate (A) without and (B) with MgO buffer layer.

roughness is calculated to be 38 and 1.6 nm for the cases without and with MgO buffer layer, respectively. Figure 3 shows the surface SEM images of the substrate without and with buffer layer. For the uncovered MgO substrate, mechanical damage striations can be observed obviously. After covering a MgO buffer layer, the surface with damage striations are replaced by one composed of uniform grains. According to the theory of crystal growth, during the growth process the molecule is preferentially absorbed toward the kinks and steps associated with dislocation (18). Especially for the mismatched system, the mechanical damage striations are apt to be nucleation points to release the strain. The vertical growth rate at damages is larger than that on other smooth areas of substrate, and then the surface

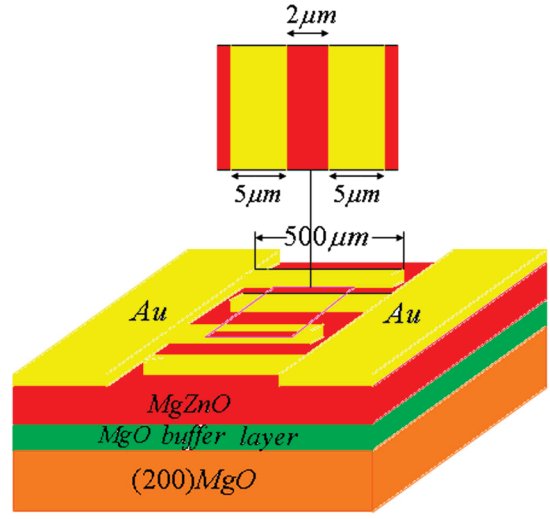

FIGURE 5. Schematic illustration of the photodetector fabricated from the high-smoothness cubic MgZnO films.

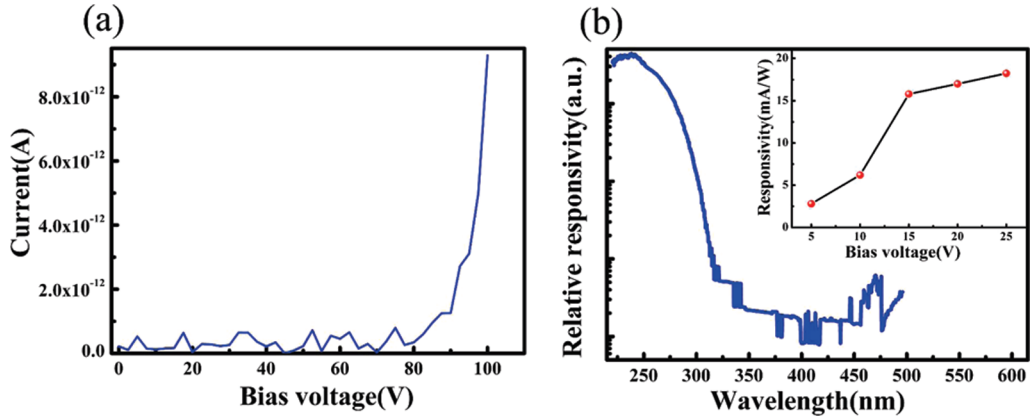

FIGURE 6. (a) Dark current as a function of bias voltage (IV) for the $Mg_xZn_{1-x}O$ photodetector. (b) Response spectrum of MgZnO solar-blind photodetector under 10 V bias; inset is the responsivity as function of bias voltage under 240 nm light illumination.

smoothness was restricted. In other words, the growth tends toward three dimension mode, which brings rough surface. After depositing a buffer layer, the mechanical damages were repaired partly. The nicks are no longer observed under SEM. The growth is in good two-dimension mode. Even at the same growth conditions, the roughness of he surface obtains improvement by 2 orders of magnitude.

Figure 4 shows the optical absorption spectra of $Mg_xZn_{1-x}O$ thin film grown directly on MgO substrate (curve A) and the one with a 25 nm MgO buffer layer (curve B). For the sample without MgO buffer, a gentle absorption edge was located at 258 nm. The band gap is fitted to be 4.85 eV from the plot of $(\alpha h\nu)^2$ as a function of photon energy ($h\nu$), as shown in the inset. For the sample with MgO buffer, the absorption edge is at 255 nm and much sharper than that without MgO buffer. The band gap of the film is 4.88 eV. To a certain extent, Sharp absorption edge means more uniform composition distribution in an alloy and sharp cutoff edge for photodetector devices.

To prove the advantage of the smooth surface for solar blind ultraviolet detection, a MSM type photodetector was fabricated on the MgZnO films, which is schematically shown in Figure 5. It consists of a 300 nm MgZnO film on MgO substrate with 25 nm MgO buffer layer, and interdigital Au electrodes were achieved by photolithography and wet etching procedure. The finger was 500 μm in length and 5 μm in width, and the spacing between the fingers is 2 μm.

Figure 6a shows the $I-V$ curve of this photodetector. The dark current reaches 0.16 pA at 15 V bias voltage. The low dark current benefits from the high crystal quality and good schottky contact. The detector shows a breakdown voltage up to 90 V. Figure 6b shows the response spectrum of the photodetector. The peak response occurred at 240 nm, and the cutoff edge is at 255 nm, in accordance with absorption edge shown in Figure 4. The maximum resposivity is 15.8 mA/W at 15 V bias, the restrict ration [R(240/400 nm)] is about 4 orders of magnitude. Here, the photodetector shows lower sub-bandgap response than our results reported earlier. The good surface smoothness is considered as an important factor. For a detector with rough surface, a lot of defects on the surface will increase the response for sub-bandgap photons. Further more, sub-bandgap light will have larger absorption probability than that in smooth films because of the increased scattering times. Therefore, the sub-bandgap responsivity is magnified though the absorption coefficient is small. For the film with smooth surface, decrease in scattering will suppress the responsivity of sub-bandgap light. It should be noted that the maximum responsivity increased from 2.8 mA/W to 15.8 mA/W with bias voltage from 5 V to 15 V, and the slope becomes gentle when the bias was over 15 V. It is a typical characteristic of schottky-type optical electronic device without internal gain, which means that an excellent schottky contact has been obtained. The good $I-V$ properties can be attributed to the tight contact between the high smooth surface and the Au electrodes.

CONCLUSIONS

Cubic $Mg_xZn_{1-x}O$ thin films with (200) orientation were deposited on MgO substrate by MOCVD. By introducing a MgO buffer layer, the surface smoothness of $Mg_xZn_{1-x}O$ thin film got great improvement from rms roughness of 38 to 1.6 nm. That the mechanical damage is repaired and covered by buffer layer is attributed to the main reason for the smoothing of the films. Schottky-type MSM photodetector was fabricated on the MgZnO thin film with low dark current 1.6×10^{-13} A. It is found that the sub-bandgap light response is efficiently suppressed compared to results reported early. It is attributed to the decrease in sub-bandgap light scattering profited from the smooth surface.

Acknowledgment. This work is supported by the Key Project of National Natural Science Foundation of China under Grant 10974197, the "973" program under Grant 2006CB604906, and the Knowledge Innovation Program of the Chinese Academy of Sciences, Grant KJCX3.SYW.W01.

REFERENCES AND NOTES

(1) Zhang, D. H.; Brodie, D. E. *Thin Solid Films* **1994**, *238*, 95.
(2) Takahashi, Y.; Kanamori, M.; Kondoh, A.; Minoura, H.; Ohya, Jpn, Y. *J. Appl. Phys.* **1994**, *33*, 6611.
(3) Studenikin, S. A.; Golego, N.; Cocivera, M. *J. Appl. Phys.* **2000**, *87*, 2413.
(4) Sharma, P.; Mansingh, A.; Sreenivas, K. *Appl. Phys. Lett.* **2002**, *80*, 553.
(5) Duboz, J. Y.; Reverchon, J. L.; Adam, D.; Damilano, B.; Grandjean, N.; Semond; Massies, J. *J. Appl. Phys.* **2002**, *92*, 9.

(6) Tut, T.; Yelboga, T.; Ulker, E.; Ozbay, E. *Appl. Phys. Lett.* **2008**, *92*, 103502.
(7) Jiang, H.; Egawa, T. *Appl. Phys. Lett.* **2007**, *90*, 121121.
(8) Kuryatkov, V. V.; Borisov, B. A.; Nikishin, S. A.; Kudryavtsev, Yu; Asomoza, R.; I.Kuchinskii, V.; Sokolovskii, G. S.; Song, D. Y.; Holtz, M. *J. Appl. Phys.* **2006**, *100*, 096104.
(9) Yang, W.; Hullavarad, S. S.; Nagaraj, B.; Takeuchi, I.; Sharma, R. P.; Venkatesan, T. *Appl. Phys. Lett.* **2003**, *82*, 3424.
(10) Tanaka, H.; Fujita, S. *Appl. Phys. Lett.* **2005**, *86*, 192911.
(11) Yu, P.; Wu, H. Z.; Xu, T. N.; Qiu, D. J.; Hu, G. J.; Dai, N. *J. Cryst. Growth* **2008**, *310*, 336–340.
(12) Sharma, A. K.; Narayan, J.; Muth, J. F.; Teng, C. W.; Jin, C.; Kvit, A.; Kolbas, R. M.; Holland, O. W. *Appl. Phys. Lett.* **1999**, *75*, 21.
(13) Ju, Z. G.; Shan, C. X.; Jiang, D. Y.; Zhang, J. Y.; Yao, B.; Zhao, D. X.; Shen, D. Z.; Fan, X. W. *Appl. Phys. Lett.* **2008**, *93*, 173505.
(14) Hullavarad, S. S.; Hullavarad, N. V.; Pugel, D. E.; Dhar, S.; Takeuchi, I.; Venkatesan, T.; Vispute, R. D. *J. Phys. D: Appl. Phys.* **2007**, *40*, 4887–4895.
(15) Vashaei, Z.; Minegishi, T.; Suzuki, H.; Hanada, T.; Cho, M. W.; Yao, T. *J. Appl. Phys.* **2005**, *98*, 054911.
(16) Wassner, T. A.; Laumer, B.; Maier, S.; Laufer, A.; Meyer, B. K.; Stutzmann, M.; Eickhoff, M. *J. Appl. Phys.* **2009**, *105*, 023505.
(17) Burton, W. K.; Cabrera, N.; Frank. Phil., F. C. *Trans. R. Soc. London, Ser. A* **1951**, *243*, 299–358.
(18) Eaglesham, D. J.; Cerullo, M. *Phys. Rev. Lett.* **1990**, *64*, 16.

AM100249A